We are IntechOpen, the world's leading publisher of Open Access books Built by scientists, for scientists

6,900
Open access books available

185,000
International authors and editors

200M
Downloads

Our authors are among the

154
Countries delivered to

TOP 1%
most cited scientists

12.2%
Contributors from top 500 universities



WEB OF SCIENCE™

Selection of our books indexed in the Book Citation Index in Web of Science™ Core Collection (BKCI)

Interested in publishing with us?
Contact book.department@intechopen.com

Numbers displayed above are based on latest data collected.
For more information visit www.intechopen.com



11

Numerical Simulation of Dense Gas-Solid Multiphase Flows Using Eulerian-Eulerian Two-Fluid Model

Teklay Weldeabzgi Asegehegn,
Matthias Schreiber and Hans Joachim Krautz
Brandenburg University of Technology Cottbus
Germany

1. Introduction

Gas-solid fluidized beds are widely applied in chemical processes such as drying, combustion, synthesis of fuels, granulation, polymerization etc. They have several advantageous properties including; excellent heat and mass transfer, nearly isothermal conditions due to intense gas-solid mixing, large gas-solid surface area, smooth transport of solids, uniform solid product in batch processes, and possibility of continuous and large-scale operations. On the other hand, these reactors have several drawbacks that provide a strong motivation for further studies and developments. These include; difficulty in scaling-up and design, erosion of vessel and internals, formation of agglomerates, non-uniform products due to non-uniform solids residence time during continuous operation, and high particle entrainment. These drawbacks are bottlenecks for practitioners to reliably design and scale-up commercial fluidized bed reactors. The main reason for this is that the gas-solid multiphase flow dynamics coupled with heat and mass transfer and chemical reactions that occur in these systems are very complex and not yet fully understood.

In bubbling gas-solid fluidized beds, bubble characteristics such as size, shape, velocity, distribution have a vital influence on the hydrodynamics of bed and hence on its performance as a chemical reactor and/or a heat exchange unit. The extent of gas-solid mixing and segregation, heat and mass transfer as well as reaction conversion are governed by the number, size and motion of bubbles passing through the bed (Kunii & Levenspiel, 1991). Therefore, fundamental understanding of the hydrodynamics of fluidized beds thereafter their heat and mass transfer as well as chemical conversion come only after a sound understanding of bubbling behaviour is achieved. However, prediction of bubble characteristics is extremely complex as bubbles can grow, coalesce, split or even disappear as they move from the distributor where they are formed to the top of the bed where they finally erupt. Moreover, bubble characteristics vary with geometric construction of the bed and operating conditions. In many applications, heat exchanger tubes are inserted to enhance the rate of heat and mass transfer and chemical conversion, control the operating temperature, promote good mixing and reduce gulf circulation of solids. In these systems, the bubbling behaviour is also strongly influenced by the geometry and arrangement of the internals (Yates et al., 1990; Hull et al., 1999; Asegehegn et al., 2011a). Therefore,

fundamental understating of the bubble hydrodynamics is necessary for better understanding of the complex gas-solid flow dynamics. This will lead to better optimize and improve the design, scale-up and operation procedure of the systems as well as to extend their use to novel applications.

Several experimental techniques have been developed for the past several decades in an attempt to measure and understand the bubble characteristics in laboratory-scale fluidized beds. Unfortunately, these laboratory-scale data do not necessarily scale-up accurately. To better understand the hydrodynamics in a commercial-scale fluidized bed reactor, it is necessary to study a vessel of that size. However, such experiments are not only prohibitive due to their capital and operational cost but also provide little information on the bubbling properties of the bed. In case of parametric studies, it is not practical or even impossible to vary the geometry and operating conditions of commercial-scale fluidized beds during experimentation. Moreover, due to the harsh environment and opaque nature of gas-solid flow structure of fluidized beds, it is difficult to observe the flow structure of the bed using many of the experimental techniques developed so far. Thus, together with the development of dedicated experimental techniques the development of fundamental hydrodynamic models is of utmost importance to achieve a better understanding of fluidization. Eventually this will lead to the improvement of existing processes, improved scale-up and the design of more efficient future processes. In recent years, together with rapid development of high performance computers and numerical algorithms, the rapid growth of interest in understanding the physical mechanisms responsible for the complex behaviour of gas-solid systems has helped to spark the development of fundamental approaches based on Computational Fluid Dynamics (CFD). Though empirical correlations are still largely used for designing gas-solid fluidized beds, these CFD models have been seen as fundamental tools in the study of the hydrodynamics and to aid in the design process of these systems. Numerical models are more flexible and less expensive specially when performing parametric studies for different bed geometries and operating conditions. Moreover, they provide extensive data for bubble characteristics for the entire cross section of the bed regardless of the complexity of bed geometry and operating conditions. However, further model development and validation of the models are still needed. It is believed that such validated CFD models can contribute to the successful understanding of bubble characteristics hence the design and optimization of these industrially relevant reactors.

Broadly speaking, there are two types of CFD models for gas-solid multiphase flow simulations that are widely applied today; namely, the Discrete Particle Model (DPM) and the Two-Fluid Model (TFM). In the DPM approach, which is based on the Eulerian-Lagrangian approach (Tsuji et al., 1993; Hoomans et al., 1996), the gas phase is treated as a continuous phase described by locally averaged Navier-Stokes equations on a computational cell scale, whereas the motion of particles is modelled as a discrete phase, described by Newton's laws of motion on an individual particle scale. A comprehensive review of the state of the Eulerian-Lagrangian model with a detailed description and governing equations as well as their application in the study of fluidized beds can be found elsewhere in the literature (e.g. Deen et al., 2007). In the TFM, which is based on the Eulerian-Eulerian approach (Anderson & Jackson, 1967), both the gas and solid phases are treated as fully interpenetrating continua. They are described by separate conservation equations for mass and momentum with appropriate interaction term between the phases included as a source terms in the conservation equations to couple the two phases.

Practically the motion of gas-particle flow systems present in fluidized beds should be expressed at least by the Eulerian-Lagrangian approach with the Newtonian equations of motion for the suspended particles. However, when the system comprises a large number of closely spaced particles, as in the case of fluidized bed, the problem is far too difficult to allow direct solution by tracking individual particles. Despite the rapid growth in computer capacity, it is only possible to track less than 10^6 particles (much less than the practical number of particles found in industrial scale fluidized beds) using the DPM. Since both CPU time and the required memory scales linear with the number of particles, it is obvious that DPM simulations of engineering size fluidized beds are beyond the capability of commercially available computer facilities within the foreseeable future. Therefore, DPM is not a natural choice for hydrodynamic modelling of gas-solid systems. For practical purposes, it is necessary to seek some way of simplifying it so that it can be described by a relatively small number of partial differential equations. One way of simplifying this problem is to replace the point mechanical and fluid mechanical variables by an appropriate locally average value of the corresponding variables to formulate the integral balances for mass, momentum and energy for a fixed control volume containing both phases. Hence describing the motion of the fluid and particles as though they were interpenetrating continua (Anderson and Jackson, 1967). In such continuum model, the equations are a generalization of the Navier-Stokes equations for interacting continua. This means that instead of knowing the positions and velocities of each particle, only the volume fraction of each phase and the average volume flow pattern are known. Though the local instantaneous value of variables vary rapidly on a scale comparable with the particle spacing the averaged variables are smoothed by averaging over regions large compared with the particle spacing but small compared with the size of complete system. The main advantage of this model is that the averaging techniques allow us to use relatively coarser grids and longer time steps so that the computational effort is significantly reduced, hence larger scale simulations can be performed, using less computation time.

In fact, the continuum model suffers from some limitations in modelling of the gas-solid flow. It does not provide information about the hydrodynamics of individual particles and thus has limitations in predicting certain discrete flow characteristics such as particle size and density effect. Nevertheless, it remains the only feasible approach for performing parametric investigation and scale-up and design studies of industrial scale systems and dense gas-solid beds (van Wachem et al., 2001; van der Hoef et al., 2008). Detail comparisons of the DPM and the TFM can be found elsewhere in the literature (e.g., Gera et al., 1998; Chiesa et al., 2005; van der Hoef et al., 2008)

2. The Eulerian two-fluid model

Most literatures give tribute to the paper by Davidson (1961) as the first to apply the concept of hydrodynamic model in fluidized beds in his analysis of a single isolated bubble rising in an unbounded fluidized bed. However, Anderson & Jackson (1967) were the first to formulate the complete CFD TFM for gas-solid multiphase flows in the mid 60's. Since then many have made significant efforts to develop detailed microbalance models to study the complex hydrodynamics of gas-fluidized beds (e.g., Gidaspow, 1994; Enwald et al., 1996; Kuipers & van Swaaij, 1998).

Owing to the continuum description of the particulate suspension, the TFM requires additional closure laws for the solid rheology. Two of the most important transport

variables that appear in the momentum equation of the solid are the solids stress tensor and solids pressure. These variables depend strongly on the collisional behaviour of the individual particles, hence difficult to express. So far, there are two types of approaches to treat these variables. The first one is commonly known as the Constant Viscosity Model (CVM) and was applied by many of the early TFM computer simulations (e.g. Gidaspow & Ettehadieh, 1983; Tsuo & Gidaspow, 1990; Kuipers et al., 1992, 1993; Enwald et al., 1996). This approach assumes a constant value for the solids viscosity obtained from some experimental and empirical correlations. The solids phase pressure, which prevents particles from reaching impossibly low values of void fraction, was assumed to depend on the solid volume fraction and it is determined from experiments. The advantage of this model is its simplicity and thus easy to implement in a computer codes. However, it is difficult to take into account the underlying characteristics of the solid phase rheology due to mutual particle collisions. The second approach makes use of the Kinetic Theory of Granular Flow (KTGF) and develops some relations as a function of the particle velocity and position (Ding & Gidaspow, 1990). One of the advantages of the KTGF is that it can give a more fundamental insight of the particle-particle interactions. Detail explanation of this model is presented in section 3.3 below.

Over the past 20 years, a large number of researchers have devoted significant effort to apply and validate the TFM based on the KTGF for different flow regimes and particle classes. For example, Boemer et al. (1997, 1998), van Wachem et al. (1998, 1999, 2001), Hulme et al. (2005), Patil et al. (2005), Lindborg et al. (2007) have been devoted to validate the model for bubble behaviour in gas-solid fluidized beds. The majority of these and other validation works are only relevant for beds without immersed tubes and to date little has been done to validate the TFM for fluidized beds with immersed obstacles. Those who performed numerical simulation using the TFM for beds with immersed tubes are mainly limited to beds with single or few tubes. Moreover, their validations involved mainly qualitative comparisons such as voidage distribution and solid circulation near the tube surface in an attempt to investigate the heat transfer coefficient or erosion characteristics of the tubes (Bouillard et al., 1989; Gamwo et al., 1999; Gustavson & Almstedt, 2000; Yurong et al., 2004; Schmidt & Renz, 2005; Gao et al., 2007). There are also attempts in validating the TFM using time-averaged bubble properties (Das Sharma & Mohan, 2003; Asegehegn et al., 2011a). Nevertheless, these are limited to only few immersed horizontal tubes.

In this chapter of the book, numerical simulations of gas-solid fluidized beds were performed using the granular TFM for beds without and with dense immersed tubes. The results of bubble properties were thoroughly analyzed and validated with experimental results obtained from pseudo-2D bed. Moreover, comparisons between 2D and 3D simulations were performed.

3. Numerical modelling using the Granular two-fluid model

3.1 Governing equations

The conservation of mass for both the gas and the solids phase can be written as:

$$\frac{\partial(\varepsilon_g \rho_g)}{\partial t} + \nabla \cdot \left(\varepsilon_g \rho_g \boldsymbol{u}_g\right) = 0 \tag{1}$$

$$\frac{\partial(\varepsilon_s \rho_s)}{\partial t} + \nabla \cdot \left(\varepsilon_s \rho_s \boldsymbol{u}_s\right) = 0 \tag{2}$$

The volume fractions are related as:

$$\varepsilon_s + \varepsilon_g = 1 \tag{3}$$

The conservation of momentum for the gas and the solids phase are described by:

$$\frac{\partial(\varepsilon_g \rho_g \boldsymbol{u}_g)}{\partial t} + \nabla \cdot \left(\varepsilon_g \rho_g \boldsymbol{u}_g \boldsymbol{u}_g\right) = \nabla \cdot \left(\boldsymbol{\tau}_g\right) - \varepsilon_g \nabla P - \beta\left(\boldsymbol{u}_g - \boldsymbol{u}_s\right) + \varepsilon_g \rho_g \boldsymbol{g} \tag{4}$$

$$\frac{\partial(\varepsilon_s \rho_s \boldsymbol{u}_s)}{\partial t} + \nabla \cdot (\varepsilon_s \rho_s \boldsymbol{u}_s \boldsymbol{u}_s) = \nabla \cdot (\boldsymbol{\tau}_s) - \varepsilon_s \nabla P - \nabla P_s + \beta\left(\boldsymbol{u}_g - \boldsymbol{u}_s\right) + \varepsilon_s \rho_s \boldsymbol{g} \tag{5}$$

3.2 Interphase momentum transfer

In the TFM the two phase are coupled through the interphase momentum transfer, hence it is one of the most important and dominant force in modelling gas-solid systems. The drag force acting on a particle in fluid–solid systems is generally represented by the product of a momentum transfer coefficient and the slip velocity ($u_g - u_s$) between the two phases. Numerous empirical correlations for calculating the momentum transfer coefficient, β, of gas-solid systems have been reported in the literature. These have been compared and validated by different researchers before, e.g. van Wachem et al. (2001), Taghipour et al. (2005), and Vejahati et al. (2009). All these researchers reported that the different drag models available gave quantitatively similar predictions of the macroscopic bed characteristic and bubble properties. As a result, the most commonly used drag model of Gidaspow (1994) was used in this work.

$$\beta = 150\frac{(1-\varepsilon_g)^2}{\varepsilon_g}\frac{\mu_g}{(d_p)^2} + 1.75\left(1-\varepsilon_g\right)\frac{\rho_g}{d_p}\left|u_g - u_s\right|, \quad if \quad \varepsilon_g \leq 0.8 \tag{6}$$

$$\beta = \frac{3}{4}C_d\frac{\varepsilon_g(1-\varepsilon_g)}{d_p}\rho_g\left|u_g - u_s\right|\varepsilon_g^{-2.65}, \qquad if \quad \varepsilon_g > 0.8 \tag{7}$$

Where,

$$C_d = \begin{cases} \frac{24}{Re_p}\left[1 + 0.15\left(Re_p\right)^{0.687}\right] & , Re_p \leq 1000 \\ 0.44 & , Re_p > 1000 \end{cases} \tag{8}$$

The particle Reynolds number is given by:

$$Re_p = \frac{\varepsilon_g \rho_g |u_g - u_s| d_p}{\mu_g} \tag{9}$$

3.3 Kinetic theory of granular flow

Almost all recent TFM of gas-solid systems used the Kinetic Theory of Granular Flow (KTGF) principle to derive the constitutive equations to describe the rheology of the particulate phase, i.e., the particulate phase viscosity and the particulate phase pressure gradient. The KTGF is basically an extension of the classical kinetic theories of non-uniform gases as described by Chapman & Cowling (1970). It was first applied to granular flows by Jenkins & Savage (1983) and Lun et al. (1984). Later Sinclair & Jackson (1989) applied this theory to model gas-solid flow in a pipe. The model was further developed and applied to dense gas-solid fluidized beds by Ding & Gidaspow (1990) and Gidaspow (1994). The

extensions were made to include the dissipation of kinetic fluctuation energy in the granular medium during mutual non-ideal particle-particle collisions due to inelastic deformation and friction of particles with the surrounding fluid.

In gas-solid flow, the interaction of the particles and the gas is restricted to a mutual drag force. Since the gas does not slip freely at the wall of the vessel, there is a gas velocity profile in fully developed flow, with the maximum velocity on the axis of the pipe, and the drag forces exerted by the gas on the particles induce a corresponding profile of particle velocity. As a result of this shearing motion the particles collide with each other, resulting in a random granular motion of particle. Thus, the instantaneous particle velocity can be decomposed into a local mean velocity and random fluctuation velocity. The random velocity fluctuations then generate an effective pressure in the particle phase, together with an effective viscosity that resists shearing of the particle assembly. Similar to the usual thermodynamic temperature in gases, a pseudo-temperature, known as the granular temperature Θ is defined as one third of the mean square of the random velocity component of the velocity, u', (Jenkins & Savage, 1983) as:

$$\Theta = \frac{1}{3}u'^2 \tag{10}$$

This granular temperature is the measure of the particle velocity fluctuation mainly due to the particle-particle collision and varies with time and position in the fluidized bed. Therefore, both the effective pressure and the effective viscosity are functions of the granular temperature. As a result, an additional conservation equation representing a balance for this kinetic energy of the random motion of the particles is required to determine the pseudo (granular) temperature distribution. This pseudo-thermal energy is generated by the working of the effective shear stresses in the particle phase, dissipated by the inelasticity of collisions between particles and conducted from place to place as a result of gradients in the particle temperature. The additional conservation equation of the particle velocity fluctuations is described by a separate conservation, the so-called granular temperature equation:

$$\frac{3}{2}\left(\frac{\partial(\varepsilon_s\rho_s\Theta)}{\partial t} + \nabla\cdot(\varepsilon_s\rho_s u_s\Theta)\right) = (-P_s I + \tau_s):\nabla u_s - \nabla\cdot q - \gamma_s - J_s \tag{11}$$

The left hand side of this equation is the net change in fluctuating energy. The first term on the right hand side is the generation of fluctuating energy due to local acceleration of the particles, which includes solid pressure and shear tensor. The second term is the diffusion of fluctuating energy. The third term on the right hand side is the dissipation of fluctuating energy due to inelastic particle-particle collision and the last term is the exchange of fluctuation energy between gas and solid phases, which accounts for the loss of granular energy due to friction with the gas.

Instead of solving the complete granular temperature equation Syamlal et al. (1993) proposed an algebraic form of the equation. They assumed a local equilibrium between generation and dissipation of the granular energy as these terms are the most dominant terms in dense regions. Thus, the convection and diffusion terms can be neglected. Boemer et al. (1997) and van Wachem et al. (2001) showed that using the algebraic form instead of the full partial differential equation hardly affects simulation results while significant computational time can be saved. By neglecting the convection and diffusion terms and retaining only the generation and the dissipation terms, Eq. 11 is reduced to:

$$0 = (-P_s I + \tau_s) : \nabla u_s - \gamma_s \tag{12}$$

For detail discussions and derivation of the kinetic theory, interested readers are referred to the book by Gidapow (1994) and papers by Jenkins & Savage (1983), Lun et al. (1984), Ding & Gidaspow (1990).

3.3.1 Gas phase stress tensor

Gases are usually assumed Newtonian fluids thus the stress tensor is modelled using the Newtonian stress-strain relation as:

$$\boldsymbol{\tau}_g = -\varepsilon_g \left[\left(\xi_g - \frac{2}{3}\mu_g \right) (\nabla \cdot \boldsymbol{u}_g) \boldsymbol{I} + \mu_g \left((\nabla \boldsymbol{u}_g) + (\nabla \boldsymbol{u}_g)^T \right) \right] \tag{13}$$

For the gas phase, the bulk viscosity ξ_g is usually set to zero while the shear viscosity μ_g is assumed to be constant.

3.3.2 Solids phase shear stress tensor

The solids phase is also assumed Newtonian and the stress tensor is given by:

$$\boldsymbol{\tau}_s = -\varepsilon_s \left[\left(\xi_s - \frac{2}{3}\mu_s \right) (\nabla \cdot \boldsymbol{u}_s) \boldsymbol{I} + \mu_s \left((\nabla \boldsymbol{u}_s) + (\nabla \boldsymbol{u}_s)^T \right) \right] \tag{14}$$

In fluidized beds the bulk and shear viscosities of the particulate phase are of the same order and thus bulk viscosity is not neglected.

Solids bulk viscosity

Solids bulk viscosity describes the resistance of particle suspension against compression. In general the model proposed by Lun et al. (1984) used and is given by:

$$\xi_s = \frac{4}{3}\varepsilon_s \rho_s d_p g_o (1+e) \sqrt{\Theta/\pi} \tag{15}$$

Solids shear viscosity

Shear viscosity represents the tangential forces due to translational and collisional interaction of particles. In general it is written as the sum of a collisional and a kinetic part:

$$\mu_{s,KTGF} = \mu_{s,col} + \mu_{s,kin} \tag{16}$$

There are several models for the shear viscosity expression in the literature. Basically all use similar expression for the collision contribution however their expression for the kinetic contribution of the solids shear viscosity differs. van Wachem et al. (2001) compared the performance of the most commonly used models and they reported that the models differ mainly in the dilute region ($\varepsilon_s < 0.3$), which is of minor importance in bubbling fluidized beds. In dense solid systems, there is no difference in the predicted solids viscosity of the models. Therefore, the model proposed by Gidaspow (1994) was used in this work.

$$\mu_{s,col} = \frac{4}{5}\varepsilon_s \rho_s d_p g_o (1+e) \sqrt{\Theta/\pi} \tag{17}$$

$$\mu_{s,kin} = \frac{1}{15}\sqrt{\Theta\pi}\rho_s d_p g_0 \varepsilon_s^2 (1+e) + \frac{1}{16}\sqrt{\Theta\pi}\rho_s d_p \varepsilon_s + \frac{10}{96}\sqrt{\Theta\pi}\frac{\rho_s d_p}{g_0(1+e)} \tag{18}$$

3.3.3 Dissipation of granular energy

The dissipation term in the fluctuating granular energy equation (Eq. 11 and 12) represents the dissipation of granular energy due to inelastic particle-particle collisions and is usually expressed by the model of Lun et al. (1984) as:

$$\gamma_s = 12(1-e^2)\frac{\varepsilon_s^2 \rho_s g_0}{d_p\sqrt{\pi}}\Theta^{3/2} \tag{19}$$

3.3.4 Radial distribution function

The radial distribution function can be interpreted as the probability of a single particle touching another particle (probability of particle collision) in the solids phase. The value of the radial distribution function varies from one at zero solids volume fractions and tends to infinity when the solids volume fraction reaches the maximum packing limit, due to constant contact of the particles. The function allows a tight control of the solids volume fraction, so that maximum packing is not exceeded and more accurate flow characteristics can be achieved. There are several empirical models for the radial distribution function and have been compared by van Wachem et al. (2001). In this work the model proposed by Ma & Ahmadi (1986) was used.

$$g_0 = 1 + 4\varepsilon_s \left\{ \frac{1+2.5\varepsilon_s+4.5904\varepsilon_s^2+4.515439\varepsilon_s^3}{\left[1-\left(\varepsilon_s/\varepsilon_{s,max}\right)^3\right]^{0.67802}} \right\} \tag{20}$$

3.3.5 Solids pressure

The solids pressure represents the normal forces due to particle-particle interactions and it prevents the solids phase from reaching unrealistic high solids volume fractions. It also helps to make the system numerically stable by converting imaginary characteristics into real ones (Kuipers et al., 1992). It is written as the sum of the kinetic and collisional term as given by Lun et al. (1984):

$$P_{s,KTGF} = \varepsilon_s \rho_s \Theta + 2g_o \varepsilon_s^2 \rho_s \Theta(1+e) \tag{21}$$

3.3.6 Frictional stresses

When particles are closely packed, as in the case of dense fluidized beds, the behaviour of the granular flow is not adequately described by kinetic theory, which assumes collisions to be binary and quasi-instantaneous. In regions with high particle volume fractions multi-particle contacts (frictional stresses) dominate the stress generation mechanism. Hence, it is necessary to include these stresses in the model. Similar to shear stress, frictional stress is composed of the frictional shear viscosity and frictional solids pressure, which includes tangential and normal frictional forces. The frictional stresses are simply added to the solid stresses from KTGF when the solids volume fraction exceeds a certain value $\varepsilon_{s,min}$, which is set to 0.6 in this work.

$$\mu_s = \mu_{s,KTGF} + \mu_{s,f} \tag{22}$$

$$P_s = P_{s,KTGF} + P_{s,f} \tag{23}$$

Here the Schaeffer (1987) model for frictional shear viscosity and the Johnson et al. (1990) model for frictional pressure were used:

$$\mu_{s,f} = \frac{P_s \sin\phi}{2\sqrt{I_{2D}}} \tag{24}$$

$$P_{s,f} = Fr\frac{(\varepsilon_s - \varepsilon_{s,min})^n}{(\varepsilon_{s,max} - \varepsilon_s)^p} \tag{25}$$

3.4 Initial and boundary conditions

The initial conditions for all simulation cases were set to the minimum fluidization condition with a bed voidage of 0.38 and bed height at minimum fluidization of 0.5 m. At the inlet the velocity inlet boundary condition with uniform superficial velocity of the gas phase was set. At the outlet the pressure outlet boundary condition was set for the mixture phase and the height of the free board was made long enough so that fully developed flow was achieved for the gas phase. At the side and tube walls the gas phase was assumed to have a no-slip boundary condition. For the particulate the partial-slip boundary condition of Johnson & Jackson (1987) was used.

$$\tau_w = \frac{\pi}{6}\sqrt{3}\phi'\frac{\varepsilon_s}{\varepsilon_{s,max}}\rho_s g_0 \sqrt{\Theta} u_{slip} \tag{26}$$

3.5 Simulation parameters and procedure

The two different bed geometries shown in Fig. 1 were used for the numerical simulations. All the dimensions of the beds were similar to the experimental setup except for the 2D simulation. For the solution the commercial CFD code ANSYS FLUENT 12.1 (ANSYS, 2009) was used. A uniform quadratic mesh with a size of 5 mm was applied with slight refinement of up to 2 mm near the tube surfaces to capture the higher velocity gradients there. The QUICK and second order upwind scheme were employed for spatial discretization of the continuity and momentum equations respectively and time was discretized using second order implicit. The Phase-Coupled SIMPLE algorithm was used for the pressure-velocity coupling. A fixed time step of 2.5 $\times 10^{-5}$ s was used. Table 1 shows additional simulation parameters that were used.

Parameter	**Value**
Gas density, kg/m^3	1.2
Gas viscosity, Pa·s	$1.79 \cdot 10^{-5}$
Particle density, kg/m^3	2500
Particle diameter, μm	246, 347
Minimum fluidization velocity, U_{mf}, m/s	0.0876, 0.144
Minimum fluidization solid volume fraction	0.62
Bed height at minimum fluidization, m	0.5
Restitution coefficient	0.95
Superficial velocity, m/s	$2U_{mf}$, $3U_{mf}$, $4U_{mf}$
Maximum particle packing limit	0.65
Specularity coefficient	0.50
Angle of internal friction, °	28.5
Time step size, s	$2.5 \cdot 10^{-5}$

Table 1. Additional simulation parameters.

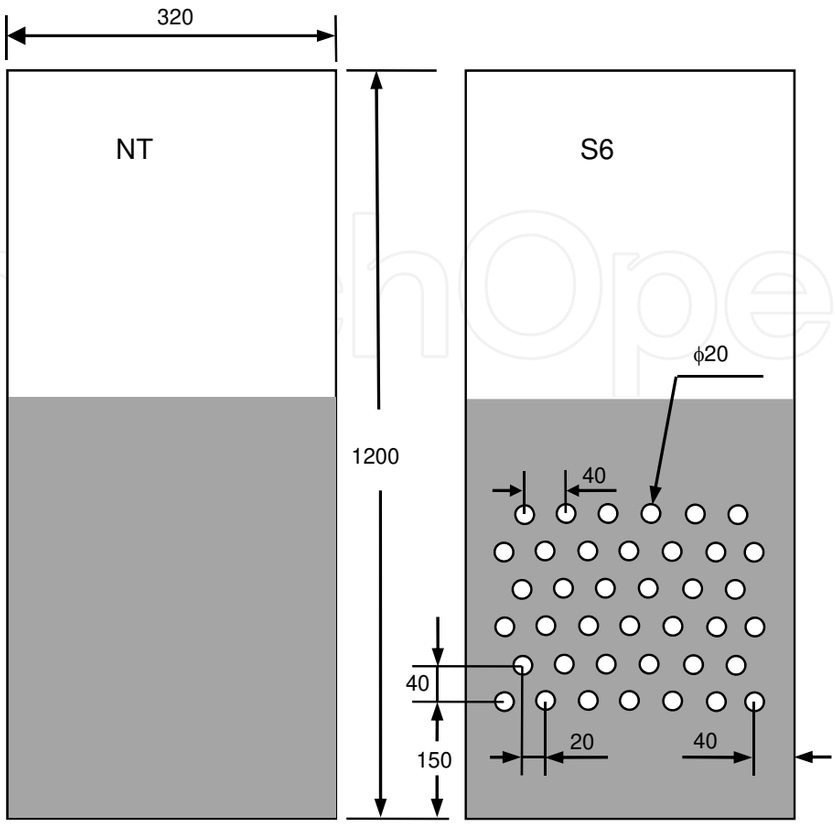


Fig. 1. Bed geometries: left - without immersed tubes (NT) and right with staggered tube arrangement (S6). All dimensions are in mm.

4. Experimental procedure

The experimental studies were performed using a specifically designed and constructed pseudo-2D fluidized bed. The bed was 0.32 m wide, 1.2 m high and 0.02 m thick and almost 2D thus allowing visual observations of bubble dynamics within the bed. The front and back sides were made of polycarbonate plastic in order to allow easy drilling of holes for assembly of the simulated tubes and allow full transparency of light. Bubble properties were calculated with the help of a Digital Image Analysis Technique (DIAT). DIAT was seen as a powerful method especially for the analysis of bubble properties as it provides rigorous and detailed information about the flow structure of the whole bed without interfering the flow dynamics. With the help of MATLAB Image Processing Toolbox, an in-house software was developed to fully automate the image acquisition and data processing procedure for the analysis of bubble properties for fluidized bed with and without immersed tubes. Detail description of the procedure was presented in our previous publication and interested readers are referred to it (Asegehegn et al., 2011b). The in-house software was developed to handle simulation results as well.

Once the bubbles are delineated and identified their projected areas A_B, horizontal and vertical coordinates of their centroids and horizontal and vertical extremes are measured. Then the bubble properties (bubble aspect ratio, diameter, rise velocity and location of the rise velocity) are calculated using equations 27 to 30 respectively.

The bubble aspect ratio, AR, is defined as:

$$AR = \mathrm{d_y}/\mathrm{d_x} \tag{27}$$

Where $\mathrm{d_y}$ and $\mathrm{d_x}$ are the vertical and horizontal extremes shown in Fig. 2.

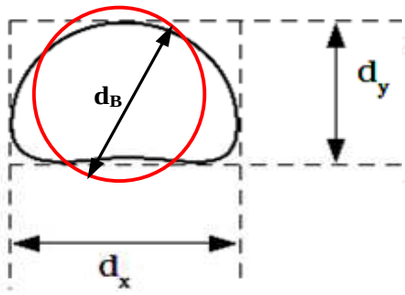


Fig. 2. Bubble dimensions.

The bubble diameter was calculated from the area equivalent $\mathrm{A_B}$ as:

$$d_B = \sqrt{4A_B/\pi} \tag{28}$$

The rise velocity was calculated from the difference in the vertical-coordinate of the centriod between consecutive time frames and dividing by the time interval between the frames.

$$u_B = \left(\mathrm{y_g(t+\Delta t) - y_g(t)}\right)/\Delta \mathrm{t} \tag{29}$$

Where $\mathrm{y_g}$ is the vertical component of the centre of gravity of the bubble, t is the time and Δt is the time delay between consecutive frames of the images, 1/50 s in this case. The velocity is attributed to the mean vertical height according to:

$$h = \left(\mathrm{y_g(t+\Delta t) + y_g(t)}\right)/2 \tag{30}$$

Once the instantaneous bubble properties at each section of the bed are calculated, a number averaging was used to calculate the time-averaged bubble properties with bed height.

$$\theta = \sum_{i=1}^{n}(\theta_i)/N \tag{31}$$

Where θ is any of the bubble property such as aspect ratio, diameter, rise velocity, and N is total number of bubble properties recorded during the total averaging time considered.

5. Results and discussions

All simulations were performed for 20 s of real flow time and the first 5 s were neglected to reduce the start-up effect. Thus, the results reported were averaged over the last 15 s of real flow time. Bubble properties were calculated from the volume fraction contours produced by the CFD software, Fig. 3.

These volume fraction contours were then analysed by the in-house code. The first step in analysing bubble properties is to discriminate the bubble from the rest of the bed. This was done by setting a solid volume fraction cut-off point to produce discriminated volume

fraction contours from the CFD code (ANSYS FLUENT 12.1) used. In the results reported in this book, a bubble was assumed to be the area with solid volume fraction of less than or equal to 0.2. There is no uniform definition of bubble boundary in literature with threshold values ranging from 0.15 to 0.30 for the solid volume fraction with 0.2 mostly used. Some sensitivity analyses performed showed that there is no significant difference in rise velocity and bubble shape with the different bubble boundaries used while the mean bubble diameter slightly varied with the threshold values (Asegehegn et al., 2011a). In this work, 50 frames per seconds were sampled to be consistent with the experimental analysis. Therefore, for the total 15 seconds of real flow time 750 frames are analysed for the statistical analysis of bubble properties. Though this was much less than the number of frames in the experimental results, considering the computational effort needed it was found to be sufficient for the statistical analysis of bubble properties.

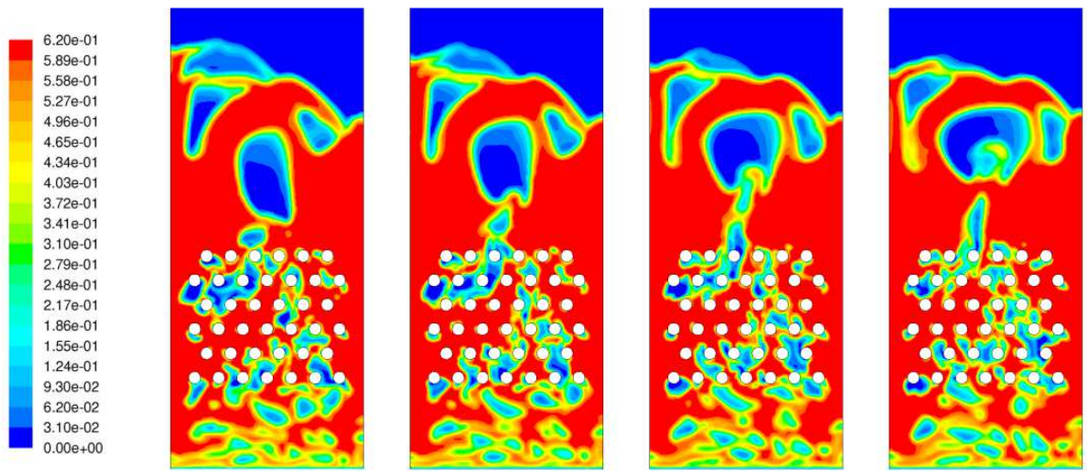


Fig. 3. Instantaneous volume fraction contour plots.

5.1 Influence of grid size

It is common practice to perform grid sensitivity analyses in order to ensure grid independent solution during numerical simulations. However, it is usually difficult to achieve grid independent solution using the granular kinetic theory as the granular theory closure equations do not give grid independent solutions with reasonable grid sizes. However, in this work a grid sensitivity analysis was performed at least to ensure the mean bubble properties are not significantly affected by the grid size used. For this purpose simulations were performed for both beds with grid sizes ranging from 2 mm to 10 mm. The results are plotted in Fig. 4 and 5 for the mean bubble diameter and mean bubble rise velocity respectively. With the exceptions of a grid size of 10 mm other sizes (5 mm, 4 mm, 2 mm) provided comparable results hence the grid size of 5 mm was selected taking into account the accuracy and computational time required.

In Table 2 the different computational times needed per one second of real flow time is presented for the different grid sizes as well as 2D and 3D simulations. All simulations were performed on a Quad-Core Intel Xeon processor (3 GHz each) workstation and a time step of 2.5×10^{-5} s was used. It can be clearly seen that the simulation time significantly increased as the grid size reduced. The difference between the NT and S6 can be attributed to the increase in number of cells in S6 as a result of the refinement near the tube surfaces.

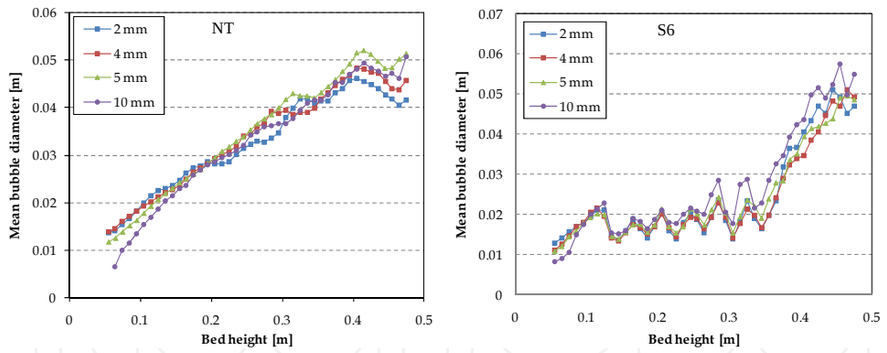


Fig. 4. Comparison of mean bubble diameter for different grid sizes.

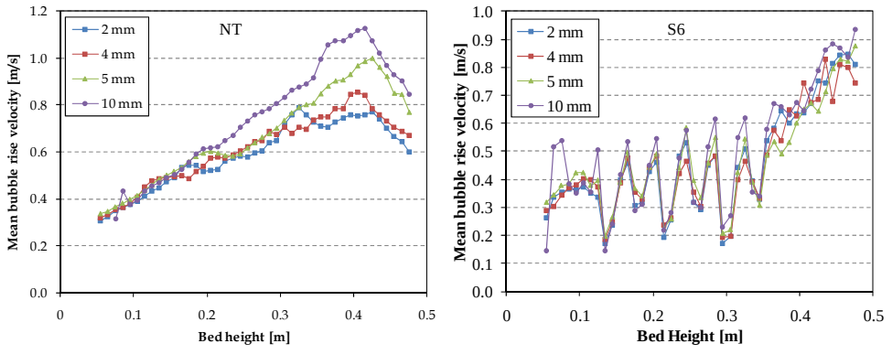


Fig. 5. Comparison of mean bubble rise velocity for different grid sizes.

Domain	Geometry	Grid size [mm]	Number of cells	Simulation time per second of real flow time [h]
2D	NT	2	96000	70
		4	24000	18
		5	15300	12
		10	3840	5
	S6	2	101838	75
		4	27694	27
		5	18469	16
		10	5190	11
3D	NT	4	120000	159
		5	61440	75
	S6	4	145705	219
		5	72924	105

Table 2. Computational time requirements for different solution domains, bed geometries and grid sizes.

5.2 Two-dimensional versus three-dimensional simulation

Generally, all practical gas-solid flows are three-dimensional (3D) in nature and numerical simulations in 3D domain should be performed to validate and study these 3D flows.

However, even with improved computational facilities, 3D simulations are still computationally prohibitive even for engineering-scale fluidized beds. Therefore, the majority of simulation studies encountered in the literature are limited to two-dimensional (2D) coordinate system to simulate 3D fluidized beds. However, there are no studies proving that 2D computations are sufficient for validation and parametric study of fluidized beds. 2D simulations are most likely to be successful in cases where the flow is presumed to be 2D, that is in cases where the variations in space and time in a given direction of the physical space are negligible compared to the variations encountered in the other directions. This is typically in the case of pseudo-2D beds, which have small depth compared to the height and width. In such cases, the particle motion can be effectively suppressed in the depth direction thus resembling 2D motion of the particles in the axial and radial directions only. Many researchers have applied 2D Cartesian simulations to model such rectangular pseudo-2D beds and found reasonable agreement between model prediction and experimental results. However, such comparisons leave an important difference between the pseudo-2D experimental beds and 2D numerical models. The front and back walls, which are neglected in the numerical model, could have considerable influence on the hydrodynamics of the fluidized beds. So far, only Li et al. (2010) have performed both 2D and 3D simulations of a pseudo-2D and compared the results with experimental measurements. They found considerable difference in the bubble rise velocity predicted by the 2D and 3D simulations while the bubble diameter predicted by both domains is generally comparable. Cammarata et al. (2003) performed simulations using 2D and 3D domains of a rectangular bed and the results of bubble diameter were compared with correlation from the literature. These authors found considerable difference of the bubble diameter predicted by the simulations. On the other hand, Peirano et al. (2001) analysed and compared simulation results of the power spectra of pressure fluctuations, bed height, and probability density function of particle volume fraction with experimental measurements. They observed a significant difference between 2D and 3D simulations and concluded that 2D simulations should be used with caution and only for sensitivity analysis. Though all the above authors concluded that 3D simulations should be preferably performed except maybe in cases where the flow is by nature 2D, they also indicate that 2D simulations could be used to conduct sensitivity analyses.

In this work, simulations were performed for two different particle sizes and two bed geometries with and without immersed horizontal tubes using 2D and 3D domains and the results were compared to experimental data obtained from pseudo-2D bed. The mean bubble diameter and rise velocity are shown in Fig. 6 and 7 respectively for the particle with mean diameter of 347 μm. Similar results were obtained for the other particle size as well but the results are not presented here to reduce redundancy. As shown in Fig. 6 the mean bubble diameter predicted by both 2D and 3D simulations are generally in very good agreement with the experimental though the 2D simulations predicted slightly smaller bubbles than the 3D. This was consistent with the results of Li et al. (2010) while Cammarata et al. (2003) reported otherwise. The results obtained from 2D simulations showed greater divergence from the experimental data with increasing bed height. Though not shown here, this was more pronounced with increasing superficial velocity. A significant difference between 2D and 3D simulations was observed in mean bubble rise velocity, Fig. 7. 2D simulations predicted much higher rise velocity than 3D simulations and significantly deviate from the experiment measurements. This was largely attributed to the wall effect. It

was believed that neglecting the front and back walls in the 2D simulations resulted in higher bubble rise velocities. In the experiment as well as 3D simulations, as a result of small bed thickness, the down flowing particles along the front and back walls increased the drag experienced by the bubbles, thus slowed the bubbles. On the other hand these walls were neglected in the 2D simulations and bubbles could move freely in the bed without experiencing the drag of down flowing particles as well as the friction of walls. Others also reported similar results, e.g. Krishna et al. (2000) and Li et al. (2010). Krishna et al. (2000) studied the influence of walls on bubble rise velocity for both gas-liquid and gas-solid systems and they reported that the rise velocity of single gas bubbles was significantly reduced as the ratio of bubble to bed width increased. Though 2D simulations have certain limitations and are physically different form the 3D flow exit in practical applications, they can provide quiet satisfactory results compared to experimental observations. It is clear that 3D simulations are more realistic and should be preferred, but with current, even in the near future, computer capacity these are far from reaching. Comparing the computational time needed for 2D and 3D simulations as shown in Table 2 above, it was found that 3D simulations are 5 to 9 times more expensive than their 2D equivalents. As an example in order to simulate 20 s of real flow time in the 2D grid with a mesh size of 5 mm using the no tube geometry 240 h (approx. 10 days) of simulation time were necessary while this was increased to 1500 h (approx. 62 days) in the case of 3D simulations. Therefore, as also deduced by Xie et al. (2008) and Cammarata et al. (2003), especially for conducting extensive parametric studies, 2D simulations remain indispensable.

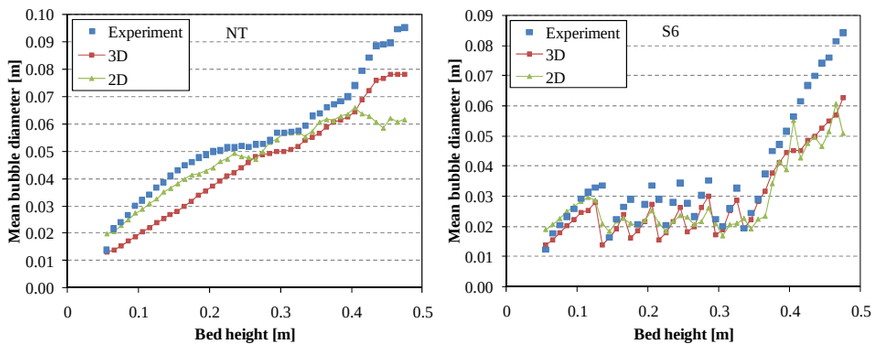


Fig. 6. Comparison of mean bubble diameter between 2D and 3D simulations, d_p = 347 μm, u=2.0U_{mf}.

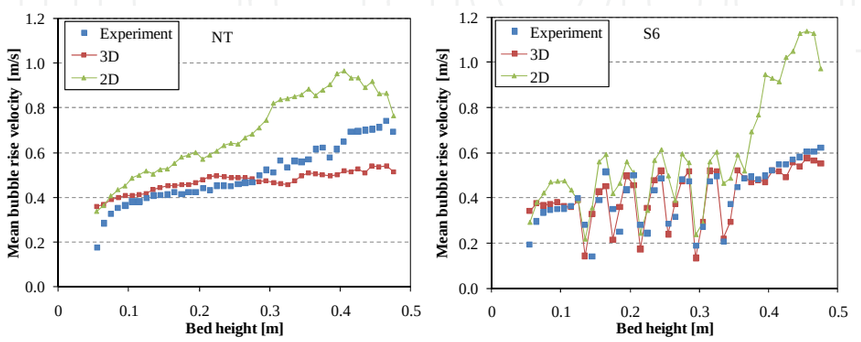


Fig. 7. Comparison of mean bubble rise velocity between 2D and 3D simulations, d_p = 347 μm, u=2.0U_{mf}.

5.3 Influence of immersed horizontal tubes

5.3.1 Bubble aspect ratio

Aspect ratio is an important characteristics of a bubble since it strongly influence the bubble's hydrodynamics. Fig. 8 shows the mean bubble aspect ratio for the two bed geometries (NT and S6) and different superficial velocities. Similar results were obtained for the second particle size and the graphs are not shown here to reduce redundancy. In general, the simulation showed good agreement with the experimental data for all geometries. For the bed without internal tubes both the simulation and experimental results predicted an increase in aspect ratio with bed height. This indicated the flattening and vertical stretching of bubbles with increasing bubble size. Generally, for beds without internal obstacles, the bubble shape was found to be nearly circular when the bubble was smaller and flattened, distorted and elongated when the bubble was bigger. Similar results were reported by Hatano et al. (1986) from experimental observations.

In the case of beds with internal horizontal tubes bubble aspect ratio was found to depend more strongly on tube geometry rather than bubble size or bed height. Bubbles were seen to elongate vertically when they moved between the tubes in a row and retained their original shape and became nearly circular when they were away from the tube rows. This resulted in oscillation of the aspect ratio in the tube bank region as shown in Fig. 8. The elongation of bubbles in the vertical direction was mainly seen as a result of the reduction in flow area and bubbles squeezed and deformed to fit the space between the tubes. As a bubble squeezed it stretched and elongated vertically as the area/volume of the bubble should at least remain the same provided that no splitting has occurred during the process. Qualitatively the simulation predicted a similar trend for fluctuations in the aspect ratio in the tube bank region, however, it predicted bubbles that were relatively circular as opposed to the corresponding experimental data. This could be associated with the no-slip boundary condition imposed on the walls for the gas phase.

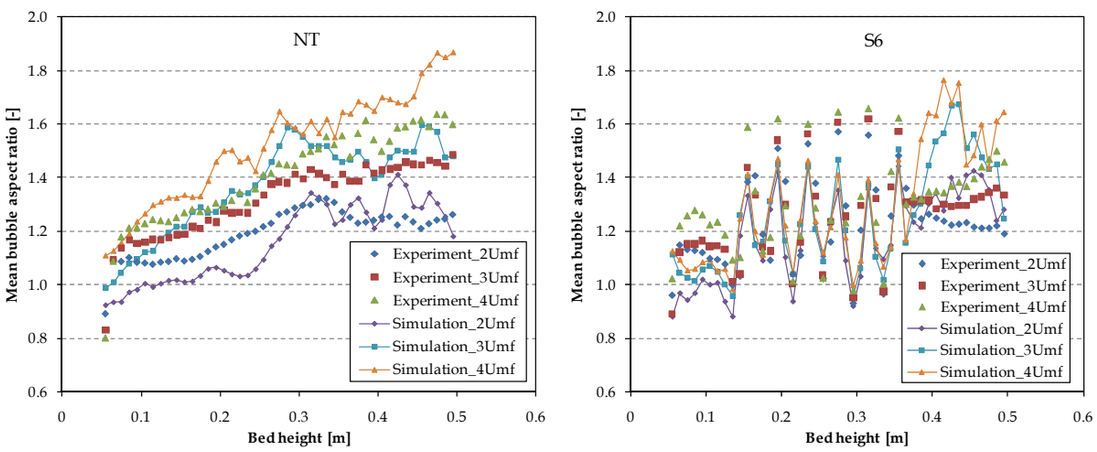


Fig. 8. Comparison of mean bubble aspect ratio between simulation results and experimental data for beds with and without immersed tubes and different superficial velocities, d_p= 246 mm and U_{mf}=0.0876 m/s.

5.3.2 Bubble size

Fig. 9 and 10 present the simulation results and comparisons with experimental data of mean bubble diameter for the two bed geometries (NT and S6) and two different particle

sizes. For beds without immersed tubes the simulation and experimental results were in very good agreement until a certain height near the eruption zone. After this height the simulation predicted no growth of bubbles while a continuous growth of bubbles was observed from the experiment.

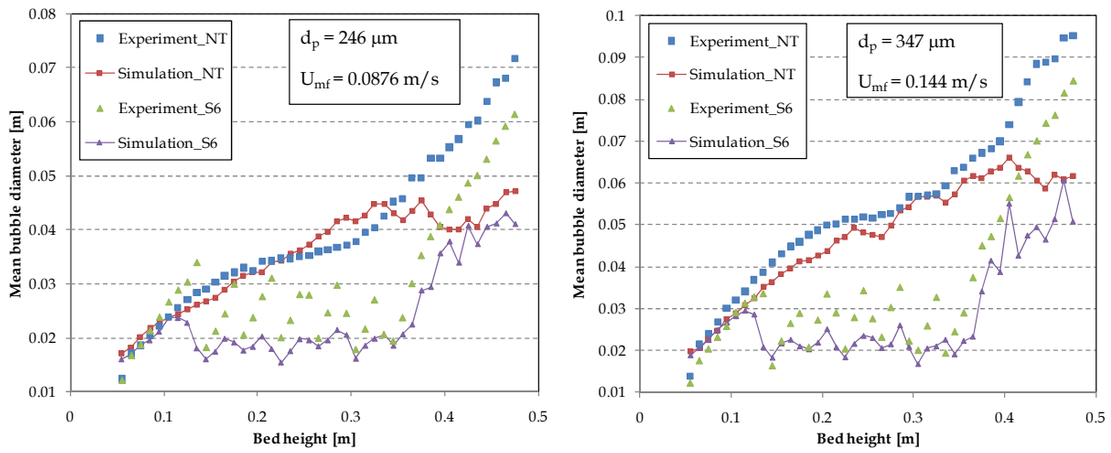


Fig. 9. Comparison of mean bubble diameter between simulation results and experimental data for beds with and without immersed tubes and two different particle sizes, $u=2U_{mf}$.

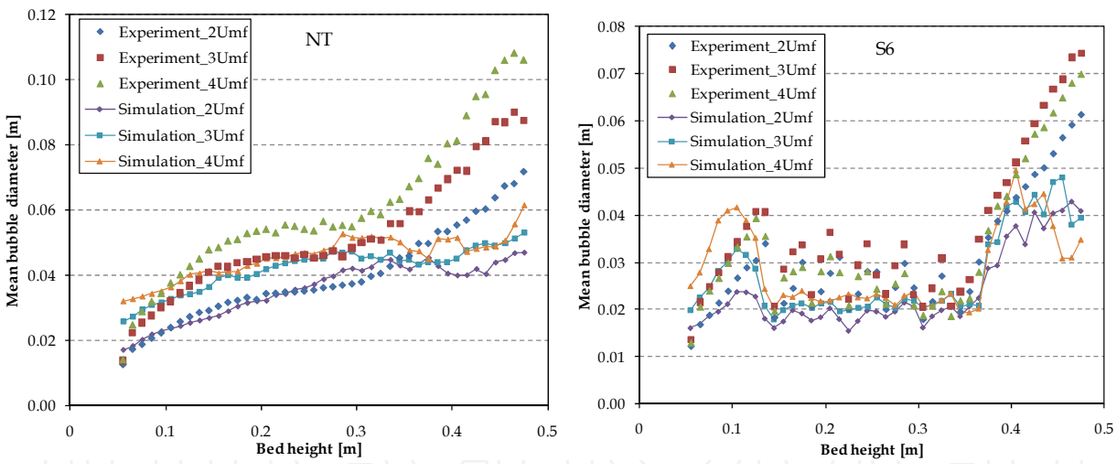


Fig. 10. Comparison of mean bubble diameter between simulation results and experimental data for beds with and without immersed tubes and different superficial velocities, d_p= 246 mm and U_{mf} = 0.0876 m/s.

In the case of beds with horizontal tubes good qualitative agreement was achieved between the simulation and experimental results for both particle sizes. However, the simulation slightly underpredicted bubble diameter in the tube bank region. This was partially attributed to the wall effect that was neglected in the numerical simulation while the experiments were performed using pseudo-2D beds. From both simulation and experiment it can be concluded that the presence of tubes resulted in higher bubble splitting and coalescence which eventually reduced the mean bubble size. Small bubbles formed at the distributor rose and grew by coalescence until they reached the first row of tubes. Upon

reaching the first row of tubes they split then grew by coalescence until they reached the second row of tubes. This continued until the last row of tubes after which bubbles rapidly grew without restriction until they finally reached the top of the bed and erupted. As shown in Fig. 10 both the simulation and experiment showed that the growth of bubbles in the tube bank region was mainly dictated by tube bank geometry rather than superficial velocity or bed height. In the tube free region, below and above the tube bank, bubble growth resembled a similar trend as in the case of the bed without immersed tubes.

5.3.3 Bubble rise velocity

Fig. 11 and 12 illustrate comparisons between simulation and experimental results for bubble rise velocities for the two bed geometries and particle sizes. For beds both with and without immersed tubes the simulation overpredicted rise velocity as compared to the experimental results and it was more pronounced at the upper part of the beds. This was largely associated with the wall effect as discussed above.

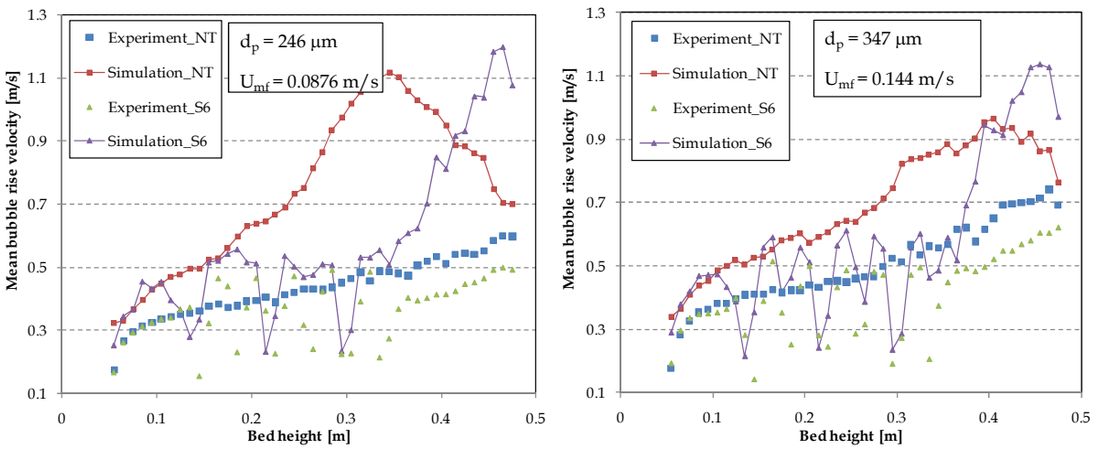


Fig. 11. Comparison of mean bubble rise velocity between simulation results and experimental data for beds with and without immersed tubes and two different particle sizes, $u=2U_{mf}$.

In the tube bank region the rise velocity was highly influenced by the presence of tubes. The reduction in bubble size due to frequent splitting in the tube bank region caused a decrease in bubble rise velocity compared to beds without internal obstacles. Both the experiment and the simulation showed higher rise velocity at the upper part of the tubes and lower rise velocity at the lower part of the tubes. The higher rise velocity seen at the upper part of the tube rows can be explained mainly due to the elongation of bubbles. As a result of elongation of a bubble and stretching the centroid of the bubble moved further in distance than it would if it were circular. This caused the centroid of the bubbles to move further in the vertical direction than they usually do. It was observed that bubbles with higher aspect ratios had higher rise velocities than those with lower aspect ratios. Hatano et al. (1986) also reported similar results for beds without internal obstacles. The reason for the lower mean rise velocity at the bottom of the tubes was due to the semi-stagnant bubbles that occurred at this location as a result of small bubble formation and splitting of bubbles into large and small daughters (Asegehegn et al. 2011a).

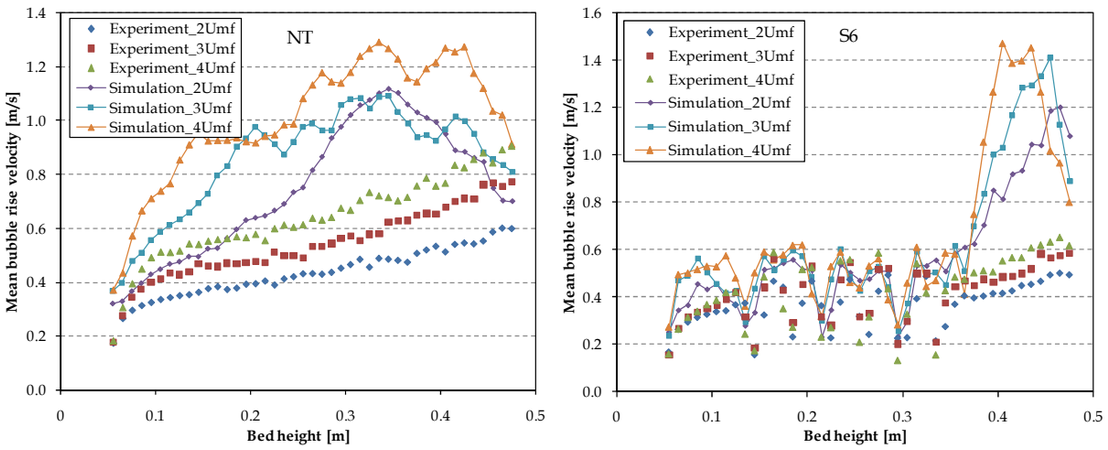


Fig. 12. Comparison of mean bubble rise between simulation results and experimental data for beds with and without immersed tubes and different superficial velocities, d_p= 246 mm and U_{mf} = 0.0876 m/s.

6. Conclusion

Numerical simulations using the Eulerian-Eulerian TFM were performed for pseudo-2D gas-solid fluidized beds with and without immersed horizontal tubes. The simulation results of bubble characteristics were compared and validated with experimental data obtained by a digital image analysis technique. From the results of this work the following conclusions can be drawn:

The two-fluid model is capable of predicting the main bubble characteristics such as bubble aspect ratio, diameter and rise velocity with and without immersed tubes. The calculated bubble properties were in general in good agreement with the experimental data.

3D simulations gave better results than 2D simulations compared with experiments. However, they are computationally expensive and 2D simulations can be successfully used for parametric study of gas-solid fluidized beds of engineering scale without losing much of the information.

The major difference between 2D and 3D simulations was observed in predicting the bubble rise velocity where 2D simulations overpredicted the bubble rise velocity compared to the corresponding 3D simulations and experimental data.

As a result of higher bubble splitting and coalescence as well as additional drag, the bubble diameter and rise velocity were lower for beds with horizontal tubes than beds without tubes. Moreover, bubble diameter and rise velocity were found to strongly depend on the tube bank geometry rather than the superficial velocity in the case of beds with dense immersed tubes while these bubble properties strongly vary with superficial velocity in the case of beds without immersed tubes.

7. Acknowledgment

The authors gratefully acknowledge the funding of this research project by the "Entrepreneurial Regions"-Initiative established by the German Federal Ministry of Education and Research and Research and COORETEC-Initiative from the Federal Ministry of Economics and Technology.

8. Nomenclature

Symbols:

A_B	Project area of a bubble, m^2
C_d	Drag coefficient
d	Diameter, m
d_x	Horizontal extreme of a bubble, m
d_y	Vertical extreme of a bubble, m
e	Coefficient of restitution
Fr	Constant in Johnson et al. (1990) friction model, N/m^2
g	Gravitational acceleration, m/s^2
g_0	Radial distribution function
I	Unit tensor
I_{2D}	Second invariant of the deviatoric stress tensor, s^{-2}
J	Granular energy transfer, $kg/m/s^3$
N	Number of bubbles, Eq. 31
n	Constant in Johnson et al. (1990) friction model
p	Constant in Johnson et al. (1990) friction model
P	Pressure, Pa
q	Diffusion of fluctuating energy, kg/s^3
Re	Reynolds number
t	Time, s
u	Velocity, m/s
u′	Fluctuating velocity, m/s

Greek Letters:

β	Interphase drag coefficient, $kg/m^3/s$
γ	Dissipation of fluctuating energy, $kg/m/s^3$
ε	Volume fraction
Θ	Granular temperature, m^2/s^2
θ	Bubble property, Eq. 31
μ	Shear viscosity, Pa·s
ξ	Bulk viscosity, Pa·s
ρ	Density, kg/m^3
τ	Shear stress tensor, N/m^2
ϕ	Angle of internal friction, °
ϕ′	Specularity coefficient

Subscripts:

B	Bubble
col	Collisional
f	Frictional
g	Gas phase
kin	Kinetic
KTGF	Kinetic Theory of Granular Flow
max	Maximum
mf	Minimum fluidization

min	Minimum
p	Particle
s	Solids phase
sl	Slip

9. References

Anderson, T.B. & Jackson, R. (1967). A Fluid Mechanical Description of Fluidized Beds Equations of Motion. *Industrial & Engineering Chemistry Fundamentals*, Vol.6, No.4, (November 1967), pp. 527-539, ISSN 0196-4313

ANSYS Inc. (2009). Eulerian Model Theory. Ansys Fluent 12.0 Theory Guide, Chapter 16.5, Lebanon.

Asegehegn, T.W.; Schreiber, M. & Krautz, H.J. (2011a). Numerical study of bubble gas-solid fluidized bed hydrodynamics: Influence of immersed horizontal tubes and data analysis. *International Journal of Chemical Reactor Engineering,* Vol. 9, A16, ISSN 1542-6580

Asegehegn, T.W.; Schreiber, M. & Krautz, H.J. (2011b). Investigation of bubble behaviour in fluidized beds with and without immersed horizontal tubes using a digital image analysis technique. *Powder Technology*, Vol. 210, No 3, (July 2011), pp. 248-260, ISSN 0032-5910

Boemer, A.; Qi, H. & Renz, U. (1997). Eulerian simulation of bubble formation at a jet in a two-dimensional fluidized bed. *International Journal of Multiphase Flow*, Vol.23, No.5, (September 1997), pp. 927-944, ISSN 0301-9322

Boemer, A.; Qi, H. & Renz, U. (1998). Verification of Eulerian Simulation of Spontaneous Bubble Formation in a Fluidized Bed. *Chemical Engineering Science*, Vol.53, No.10, (May 1998), pp. 1835-1846, ISSN 0009-2509

Bouillard, J.X.; Lyczkowski, R.W. & Gidaspow D. (1989). Porosity distributions in a fluidized bed with an immersed obstacle. *AIChE Journal*, Vol.35, No.6, (June 1989), pp. 908-922, ISSN 0001-1541

Cammarata, L.; Lettieri, P.; Micale, G.D.M.; & Colman, D. 2D and 3D CFD simulations of bubbling fluidized beds using Eulerian-Eulerian models. *International Journal of Chemical Reactor Engineering,* Vol. 1, A48., ISSN 1542-6580

Chapman, S. & Cowling, T.G. (1970). *The mathematical theory of non-uniform gases*, Cambridge University Press, ISBN 978-052-1408-44-8, Cambridge, UK

Chiesa, M., Mathiesen, V., Melheim, & Halvorsen, B. (2005). Numerical simulation of particulate flow by the Eulerian-Lagrangian and Eulerian-Eulerian approach with application to a fluidized bed. *Computer & Chemical Engineering*, Vol. 29, No. 2, (January 2005), pp. 291-304, ISSN 0098-1354

Das Sharma, S.K. & Mohan, R. (2003). Numerical study of the influence of horizontal tube banks on the hydrodynamics of a dense gas-solid bubbling fluidized bed. *International Journal of Chemical Reactor Engineering*, Vol.1, A26, ISSN 1542-6580

Davidson, J.F. (1961). Symposium on fluidization-discussion. *Transactions of the Institution of Chemical Engineers*, Vol. 39, pp. 230-232 ISSN 0371-7496

Deen, N.G.; van Sint Annaland, M.; van der Hoef, M.A. & Kuipers, J.A.M. (2007). Review of discrete particle modeling of fluidized beds. *Chemical Engineering Science*, Vol.62, No.1-2, (January 2007), pp. 28-44, ISSN 0009-2509

Ding, J. & Gidaspow, D. (1990). A bubbling fluidization model using kinetic theory of granular flow. *AIChE Journal*, Vol.36, No.4, (June 1990), pp. 523-538, ISSN 0001-1541

Enwald, H.; Peirano, E. & Almstedt, A.E. (1996). Eulerian two-phase flow theory applied to fluidization. *International Journal of Multiphase Flow*, Vol.22, Suppl.1, (December 1996), pp. 21-66, ISSN 0301-9322

Gamwo, I.K.; Soong, Y. & Lyczkowski, R.W. (1999). Numerical simulation and experimental validation of solids flows in a bubbling fluidized bed. *Powder Technology*, Vol.103, No.2, (Juli 1999), pp. 117-129, ISSN 0032-5910

Gao, W.M.; Kong, L.X. & Hodgson, P.D. (2007). Computational simulation of gas flow and heat transfer near an immersed object in fluidized beds. *Advances in Engineering Software*, Vol.38,No.11-12, (November-December 2007), pp. 826-834, ISSN 0965-9978

Gera, D., Gautam, M., Tsuji, Y., Kawaguchi, T. & Tanaka, T. (1998). Computer simulation of bubbles in large-particle fluidized beds. *Powder Technology*, Vol. 98, No. 1 , (July 1998), pp. 38-47, ISSN 0032-5910

Gidaspow, D. (1994). *Multiphase flow and fluidization: Continuum and kinetic theory descriptions*, Academic Press, ISBN 978-012-2824-70-8, Boston, USA

Gidaspow, D. & Ettehadieh, B. (1983), Fluidization in two-dimensional beds with a jet. 2. hydrodynamic modeling. *Industrial & Engineering Chemistry Fundamentals*, Vol.22, No.2, (May 1983), pp. 193-201, ISSN 0196-4313

Gustavsson, M. & Almstedt, A.E. (2000). Numerical simulation of fluid dynamics in fluidized beds with horizontal heat exchanger tubes. *Chemical Engineering Science*, Vol.55, No.4, (February 2000), pp. 857-866, ISSN 0009-2509

Hatano, H.; Khattab, I.A.H.; Nakamura, K. & Ishida, M. (1986). Spatiotemporal measurement of bubble properties in free-bubbling fluidized beds. *Journal of Chemical Engineering of Japan*, Vol.19, No.5, (September 1986), pp. 425-430, ISSN 0021-9592

Hoomans, B.P.B.; Kuipers, J.A.M.; Briels, W.J. & van Swaaij, W.P.M. (1996). Discrete particle simulation of bubble and slug formation in a two-dimensional gas-fluidized bed: A hard-sphere approach. *Chemical Engineering Science*, Vol.51, No.1, (January 1996), pp. 99-118, ISSN 0009-2509

Hull, A.S.; Chen, Z.; Fritz, J.W. & Agarwal, P.K. (1999). Influence of horizontal tube banks on the behavior of bubbling fluidized beds: 1. bubble hydrodynamics. *Powder Technology*, Vol.103, No.3, (July 1999), pp. 230-242, ISSN 0032-5910

Hulme. I.; Clavelle, E.; van der Lee, L. & Kantzas, A. (2005). CFD modeling and validation of bubble properties for a bubbling fluidized bed. *Industrial & Engineering Chemistry Research*, Vol.44, No.12, (May 2005), pp. 4254-4266, ISSN 0888-5885

Jenkins, J.T. & Savage, S.B. (1983). A Theory for the rapid flow of identical, smooth, nearly elastic, spherical particles. *Journal of Fluid Mechanics*, Vol.130, pp. 187-202, ISSN 0022-1120

Johnson, P.C.; Nott, P. & Jackson, R. (1990). Frictional-collisional equations of motion for particulate flows and their application to chutes. *Journal of Fluid Mechanics*, Vol.210, pp. 501-535, ISSN 0022-1120

Johnson, P.C. & Jackson, R. (1987). Frictional-collisional constitutive relations for granular materials, with application to plane shearing. *Journal of Fluid Mechanics*, Vol.176, pp. 67-93, ISSN 0022-1120

Krishna, R.; van Baten J.M.; Urseanu, M.I. & Ellenberger, J. (2000). Rise velocity of single circular-cap bubbles in two-dimensional beds of powders and liquids. *Chemical Engineering and Processing*, Vol.39, No.5, (September 2000), pp. 433-440, ISSN 0255-2701

Kuipers, J.A.M. & van Swaaij W.P.M. (1998). Computational fluid dynamics applied to chemical reaction engineering. *Advances in Chemical Engineering*, Vol.24, pp. 227-328

Kuipers, J.A.M.; van Duin K.J.; van Beckum, F.P.H. & van Swaaij, W.P.M. (1992). A numerical model of gas-fluidized beds. *Chemical Engineering Science*, Vol.47, No.8, (June 1992), pp. 1913-1924, ISSN 0009-2509

Kuipers, J.A.M.; van Duin K.J.; van Beckum, F.P.H. & van Swaaij, W.P.M. (1993). Computer simulation of the hydrodynamics of a two-dimensional gas-fluidized bed. *Computers & Chemical Engineering*, Vol.17, No.8, (August 1993), pp. 839-858, ISSN 0098-1354

Kunii, D. & Levenspiel, O. (1991). *Fluidization Engineering, 2nd ed.*, Butterworth-Heineman, ISBN 978-040-9902-33-4, Boston, USA

Li, T.; Grace, J.R. & Bi, X. (2010). Study of wall boundary condition in numerical simulations of bubbling fluidized beds. *Powder Technology*, Vol.203, No.3, (November 2010), pp. 447-457, ISSN 0032-5910

Lindborg, H.; Lysberg, M. & Jakobsen, H.A. (2007). Practical validation of the two-fluid model applied to dense gas–solid flows in fluidized beds. *Chemical Engineering Science*, Vol.62, No.21, (Nove,ber 2007), pp. 5854-5869, ISSN 0009-2509

Lun, C.K.K.; Savage, S.B.; Jeffrey, D.J. & Chepurniy, N. (1984). Kinetic theories for granular flow: Inelastic particles in couette flow and slightly inelastic particles in a general flow field. *Journal of Fluid Mechanics*, Vol.140, pp. 223-256, ISSN 0022-1120

Ma, D. & Ahmadi, G. (1986). An equation of state for dense rigid sphere gases. *Journal of Chemical Physics*, Vol.84, No.6, pp. 3449-3450, ISSN 0021-9606

Patil, D.J.; van Sint Annaland, M. & Kuipers, J.A.M. (2005). Critical comparison of hydrodynamic models for gas-solid fluidized beds - Part II: Freely bubbling gas-solid fluidized beds. *Chemical Engineering Science*, Vol.60, No.1, (January 2005), pp. 73-84, ISSN 0009-2509

Peirano, E.; Delloume, V. & Leckner B. (2001).Two- or three- dimensional simulations of turbulent gas-solid flows applied to fluidization. *Chemical Engineering Science*, Vol. 56, No. 16, (August 2001), pp. 4787-4799, ISSN 0009-2509

Schaeffer, D.G. (1987). Instability in the evolution equations describing incompressible granular flow. *Journal of Differential Equations*, Vol.66, No.1, (January 1987), pp. 19-50, ISSN 0022-0396

Schmidt, A. & Renz, U. (2005). Numerical prediction of heat transfer between a bubbling fluidized bed and an immersed tube bundle. *Heat Mass Transfer*, Vol.41, No.3, pp. 257-270, ISSN 0947-7411

Sinclair, J.L. & Jackson, R. (1989). Gas-particle flow in a vertical pipe with particle-particle interactions. *AIChE Journal*, Vol.35, No.9, September (1989),pp. 1473-1486, ISSN 0001-1541

Syamlal, M.; Rogers, W. & O'Brien, T.J. (1993). *MFIX Documentation: Theory guide*. National Technical Information Service, DOE/METC-94/1004, Springfield, USA

Taghipour, F.; Ellis, N. & Wong, C. (2005). Experimental and computational study of gas-solid fluidized bed hydrodynamics. *Chemical Engineering Science*, Vol.60, No.24, (December 2005), pp. 6857-6867, ISSN 0009-2509

Tsuji, Y.; Kawaguchi, T. & Tanaka, T. (1993). Discrete particle simulation of two-dimensional fluidized bed. *Powder Technology*, Vol.77, No.1, (October 1993), pp. 79-87, ISSN 0032-5910

Tsuo, Y. & Gidaspow, D. (1990). Computation of flow patterns in circulating fluidized beds. *AIChE Journal*, Vol.36, No.6, (June 1990), pp. 885-896, ISSN 0001-1541

van der Hoef, M.A.; van Sint Annaland, M.; Deen, N.G. & Kuipers, J.A.M. (2008). Numerical simulation of dense gas-solid fluidized beds: A multiscale modeling strategy. *Annual Review of Fluid Mechanics*, Vol.40, pp. 47-70, ISSN 0066-4189

van Wachem, B.G.M.; Schouten, J.C.; Krishna, R. & van den Bleek, C.M. (1998). Eulerian simulation of bubbling behaviour in gas-solid fluidized beds. *Computers and Chemical Engineering*, Vol.22, Suppl.1, (March 1998), pp. S299-S306, ISSN 0098-1354

van Wachem, B.G.M.; Schouten, J.C.; Krishna, R. & van den Bleek, C.M. (1999). Validation of the Eulerian simulated dynamic behaviour of gas-solid fluidized beds. *Chemical Engineering Science*, Vol.54, No.13-14, (July 1999), pp. 2141-2149, ISSN 0009-2509

van Wachem, B.G.M.; Schouten, J.C.; van den Bleek, C.M.; Krishna, R. & Sinclair, J.L. (2001). Comparative analysis of CFD models of dense gas-solid systems. *AIChE Journal* Vol.47, No.5, (May 2001), pp. 1035-1051, ISSN 0001-1541

Vejahati, F.; Mahinpey, N.; Ellis, N. & Nikoo, M.B. (2009). CFD simulation of gas-solid bubbling fluidized bed: A new method for adjusting drag law. *The Canadian Journal of Chemical Engineering*, Vol.87, No.1, (February 2009), pp. 19-30, ISSN 1939-019X

Xie, N.; Battaglia, F. & Pannala, S. (2008). Effects of using two- versus three-dimensional computational modeling of fluidized beds: Part 1, Hydrodynamics. *Powder Technology*, Vol.182, No.1, (February 2008), pp. 1-13, ISSN 0032-5910

Yates, J.G.; Ruiz-Martinez, R.S. & Cheesman, D.J. (1990). Prediction of size in a fluidized bed containing horizontal tubes. *Chemical Engineering Science*, Vol.45, No.4, pp. 1105-1111, ISSN 0009-2509

Yurong, H.; Huilin, L.; Qiaoqun, S.; Lidan, Y.; Yunhua, Z.; Gidaspow, D. & Bouillard, J. (2004). Hydrodynamics of gas-solid flow around immersed tubes in bubbling fluidized beds. *Powder Technology*, Vol.145, No.2, (July 2004), pp. 88-105, ISSN 0032-5910



Computational Simulations and Applications

Edited by Dr. Jianping Zhu

ISBN 978-953-307-430-6
Hard cover, 560 pages
Publisher InTech
Published online 26, October, 2011
Published in print edition October, 2011

The purpose of this book is to introduce researchers and graduate students to a broad range of applications of computational simulations, with a particular emphasis on those involving computational fluid dynamics (CFD) simulations. The book is divided into three parts: Part I covers some basic research topics and development in numerical algorithms for CFD simulations, including Reynolds stress transport modeling, central difference schemes for convection-diffusion equations, and flow simulations involving simple geometries such as a flat plate or a vertical channel. Part II covers a variety of important applications in which CFD simulations play a crucial role, including combustion process and automobile engine design, fluid heat exchange, airborne contaminant dispersion over buildings and atmospheric flow around a re-entry capsule, gas-solid two phase flow in long pipes, free surface flow around a ship hull, and hydrodynamic analysis of electrochemical cells. Part III covers applications of non-CFD based computational simulations, including atmospheric optical communications, climate system simulations, porous media flow, combustion, solidification, and sound field simulations for optimal acoustic effects.

How to reference

In order to correctly reference this scholarly work, feel free to copy and paste the following:

Teklay Weldeabzgi Asegehegn, Matthias Schreiber and Hans Joachim Krautz (2011). Numerical Simulation of Dense Gas-Solid Multiphase Flows Using Eulerian-Eulerian Two-Fluid Model, Computational Simulations and Applications, Dr. Jianping Zhu (Ed.), ISBN: 978-953-307-430-6, InTech, Available from: http://www.intechopen.com/books/computational-simulations-and-applications/numerical-simulation-of-dense-gas-solid-multiphase-flows-using-eulerian-eulerian-two-fluid-model

INTECH
open science | open minds

InTech Europe
University Campus STeP Ri
Slavka Krautzeka 83/A
51000 Rijeka, Croatia
Phone: +385 (51) 770 447
Fax: +385 (51) 686 166
www.intechopen.com

InTech China
Unit 405, Office Block, Hotel Equatorial Shanghai
No.65, Yan An Road (West), Shanghai, 200040, China
中国上海市延安西路65号上海国际贵都大饭店办公楼405单元
Phone: +86-21-62489820
Fax: +86-21-62489821

© 2011 The Author(s). Licensee IntechOpen. This is an open access article distributed under the terms of the Creative Commons Attribution 3.0 License, which permits unrestricted use, distribution, and reproduction in any medium, provided the original work is properly cited.

IntechOpen

IntechOpen